

This discussion paper is/has been under review for the journal Atmospheric Chemistry and Physics (ACP). Please refer to the corresponding final paper in ACP if available.

OH regeneration from methacrolein oxidation investigated in the atmosphere simulation chamber SAPHIR

H. Fuchs¹, I.-H. Acir¹, B. Bohn¹, T. Brauers¹, H.-P. Dorn¹, R. Häsel¹,
 A. Hofzumahaus¹, F. Holland¹, M. Kaminski¹, X. Li¹, K. Lu^{1,*}, A. Lutz², S. Nehr^{1,**},
 F. Rohrer¹, R. Tillmann¹, R. Wegener¹, and A. Wahner¹

¹Institute of Energy and Climate Research, IEK-8: Troposphere, Forschungszentrum Jülich GmbH, Jülich, Germany

²Institute of Chemistry and molecular Biology, Göteborg University, Göteborg, Sweden

* now at: College of Environmental Sciences and Engineering, Peking University, Beijing, China

** now at: Verein Deutscher Ingenieure e.V., Kommission Reinhaltung der Luft, Düsseldorf, Germany

Received: 24 January 2014 – Accepted: 18 February 2014 – Published: 25 February 2014

Correspondence to: H. Fuchs (h.fuchs@fz-juelich.de)

Published by Copernicus Publications on behalf of the European Geosciences Union.

5197

Abstract

Hydroxyl radicals (OH) are the most important reagent for the oxidation of trace gases in the atmosphere. OH concentrations measured during recent field campaigns in isoprene rich environments were unexpectedly large. A number of studies showed that unimolecular reactions of organic peroxy radicals (RO₂) formed in the initial reaction step of isoprene with OH play an important role for the OH budget in the atmosphere at low mixing ratios of nitrogen monoxide (NO) of less than 100 pptv. It has also been suggested that similar reactions potentially play an important role for RO₂ from other compounds. Here, we investigate the oxidation of methacrolein (MACR), one major oxidation product of isoprene, by OH in experiments in the simulation chamber SAPHIR under controlled atmospheric conditions. The experiments show that measured OH concentrations are approximately 50 % larger than calculated by current chemical models for conditions of the experiments (NO mixing ratio of 90 pptv). The analysis of the OH budget reveals a so far unaccounted OH source, which is correlated with the production rate of RO₂ radicals from MACR. In order to balance the measured OH destruction rate, (0.77 ± 0.3) OH radicals need to be additionally reformed from each OH that has reacted with MACR. The strong correlation of the missing OH source with the production of RO₂ radicals is consistent with the concept of OH formation from unimolecular isomerization and decomposition reactions of RO₂. The comparison of observations with model calculations gives a lower limit of 0.03 s⁻¹ for the reaction rate constant, if the OH source is attributed to an isomerization reaction of one RO₂ species formed in the MACR+OH reaction as suggested in literature. This fast isomerization reaction would be competitive to the reaction of this RO₂ species with minimum 150 pptv NO.

1 Introduction

Isoprene (2-methyl-1,3-butadiene) is the most abundant nonmethane hydrocarbon that is being emitted by the biosphere and predominantly removed by oxidation with atmospheric hydroxyl radicals (OH) (Guenther et al., 2012). Unexpectedly large OH concentrations that cannot be explained by the current knowledge of atmospheric chemistry have been found in several field campaigns (Carslaw et al., 2001; Tan et al., 2001; Kuhn et al., 2007; Ren et al., 2008; Lelieveld et al., 2008; Hofzumahaus et al., 2009; Lu et al., 2012, 2013; Stone et al., 2010; Whalley et al., 2011; Wolfe et al., 2011) for high loads of OH reactants (often dominated by isoprene) and low concentrations of nitrogen monoxide (NO). As a potential explanation for the high OH concentrations, reformation of OH radicals from unimolecular reactions of organic peroxy radicals (RO₂) that result from the reaction of isoprene with OH have been suggested (Peeters et al., 2009; Peeters and Müller, 2010; da Silva et al., 2010). The proposed reactions involve 1,5-H- and 1,6-H-shift reactions followed by decomposition of specific isoprene RO₂ isomers and compete with the well-known OH reformation via reaction of HO₂ with NO. This reaction scheme has been applied, in order to explain high levels of OH radicals, using reaction rate constants that were derived from quantum chemical calculations (Taraborrelli et al., 2012). A laboratory study investigated the products yields of the proposed reactions (Crounse et al., 2011; Wolfe et al., 2012) and direct OH measurements in experiments in the atmosphere simulation chamber SAPHIR gave evidence for OH regeneration from isoprene RO₂ without involvement of NO (Fuchs et al., 2013). Results from these experimental studies are consistent with the RO₂ isomerization reaction scheme, but also showed that isomerization reaction rate constants are smaller than originally calculated (Peeters and Müller, 2010). Thus, OH regeneration from isoprene peroxy radicals alone cannot explain elevated OH concentrations found in field campaigns. Therefore, the question arises, if unimolecular RO₂ reactions from the oxidation products of isoprene may also enhance atmospheric OH.

5199

Methacrolein (2-methylpropenal) is one of the major first-generation products of the gas-phase oxidation of isoprene by OH with a yield of approximately 20–30 % for atmospheric conditions (Tuazon and Atkinson, 1990; Galloway et al., 2011). Methacrolein (MACR) is further oxidized by OH in the atmosphere producing hydroxyacetone, methylglyoxal, and formaldehyde (Galloway et al., 2011). Similar unimolecular reactions of RO₂ as for isoprene, which may produce additional OH, have also been suggested for MACR (Peeters et al., 2009; Crounse et al., 2012; Asatryan et al., 2010; da Silva, 2012). Recently, the product distribution from the MACR plus OH reaction for various NO concentrations has been investigated in a laboratory study accompanied by quantum chemical calculations (Crounse et al., 2012). This inferred a new reaction pathway, in which hydroxyacetone is formed from a reaction pathway that is independent of the level of NO. This would be consistent with a fast unimolecular RO₂ reaction, because hydroxyacetone has so far only been known as a product of the reaction of RO₂ with NO. The new reaction path is attributed to a 1,4-H-shift isomerization reaction and implies reformation of OH as co-product (Crounse et al., 2012), but OH concentrations were not directly measured in that study.

Here, we present the investigation of the photo-oxidation of MACR by OH at controlled atmospheric conditions in the simulation chamber SAPHIR in the presence of approximately 90 pptv NO. Measurements of all relevant trace gas concentrations, including OH, hydroperoxy (HO₂) and RO₂ radicals, and the OH lifetime allow a detailed analysis of the OH budget. Recently proposed reaction pathways are tested by comparing time series of measurements with model calculations.

2 Methods

2.1 Simulation experiment in SAPHIR

Experiments were conducted in the atmosphere simulation chamber SAPHIR in Jülich, Germany. The chamber allows to investigate the photochemical oxidation of organic

5200

compounds at atmospheric conditions with respect to temperature, pressure, radiation and concentrations of trace gases and radicals. Experiments for this study were similar to those that were performed to investigate the oxidation of isoprene by OH (Fuchs et al., 2013).

5 The outdoor SAPHIR chamber is made of a double wall Teflon (FEP) film of cylindrical shape (length 18 m, diameter 5 m, volume 270 m³). Details of the chamber have been described earlier (Rohrer et al., 2005; Bohn et al., 2005; Schlosser et al., 2009). It is equipped with a shutter system, which can be opened to expose the chamber air to natural sunlight. The FEP film has a high transmittance for the entire spectrum of solar
10 radiation (Bohn et al., 2005). Slight overpressure prevents leakage of ambient air into the chamber. The chamber air is mixed from evaporated liquid nitrogen and oxygen of highest purity (Linde, purity > 99.99990 %). During all experiments reported here, a fan ensured fast mixing of the chamber air (mixing time < 2 min). Replenishment of chamber air, which is lost due to small leakages and consumption by instruments, leads to
15 a dilution of trace gases with a rate of approximately 4 % h⁻¹.

The experiments aimed to simulate conditions like those found during field experiments (Lu et al., 2012, 2013), when unexpectedly large OH concentrations were measured. At the beginning of the experiment, the dark chamber only contained clean synthetic air. The water vapour mixing ratio was increased by flushing water vapour from
20 boiling Milli-Q-water into the chamber in the dark, until the relative humidity reached approximately 80 %. Then the shutter system was opened to expose the chamber to sunlight. Ozone produced from a silent discharge ozoniser was added resulting in a mixing ratio of approximately 50 ppbv. After this initial phase ("zero air" (ZA)-phase) of the experiment (duration 2 h), MACR was injected several times with a time-lag of
25 2 h (maximum mixing ratio up to 14 ppbv). The experiment was performed three times in a similar way (Table 1).

The major primary source for OH in the chamber is photolysis of nitrous acid (HONO), which is released from the Teflon film depending on temperature, relative humidity, and strength of radiation (Rohrer et al., 2005). HONO photolysis is also

5201

the major source of nitrogen oxides. In addition, acetaldehyde and formaldehyde are formed with a rate of approximately 200 pptv h⁻¹ during these experiments. The OH reactivity is on the order of (1–2) s⁻¹ in the absence of additional OH reactants, which can be partly explained by the presence of NO, NO₂, formaldehyde (HCHO) and acetaldehyde (CH₃CHO). RO₂ radicals of approximately (1–2) × 10⁸ cm⁻³ were immediately
5 formed in the humidified clean air when the chamber roof was opened. They were partly formed by photolytic processes. This is evident from reference experiments with CO, in which the RO₂ radical concentrations persisted even though OH was completely scavenged by excess CO. Sources of trace gases and radicals can be well-parameterized
10 from reference experiments, but except for the production of HONO they played only a minor role for the experiments after MACR had been injected.

2.2 Instrumentation

Trace gas and radical concentrations were measured by instruments listed in Table 2. A laser induced fluorescence instrument (LIF) was used to measure OH, HO₂, and RO₂
15 concentrations simultaneously in three parallel measurement cells. RO₂ and HO₂ are detected via their conversion to OH involving reactions with NO. The signal of the HO₂ detection includes a small fraction of specific RO₂ species, which can be partly converted to OH on the same time-scale (Fuchs et al., 2011). Instrument parameters were optimized to minimize this interference. For RO₂, the conversion efficiency is assumed
20 to be small, if their conversion to OH requires more than two reactions with NO (like for acyl peroxy radicals), because of the short residence time between NO addition and OH detection in the instrument (Fuchs et al., 2008).

OH was also detected by a Differential Optical Absorption Spectrometer (DOAS) during two of the three experiments. As previously shown, measurements of both instruments (LIF and DOAS) agreed within their uncertainties during experiments in SAPHIR
25 that were performed for the investigation of the oxidation of various organic compounds including MACR (Schlosser et al., 2007, 2009; Fuchs et al., 2012). This indicates that OH measurements were not affected by unknown interferences.

5202

The chemical lifetime of OH was measured applying a combination of flash photolysis producing OH by ozone photolysis at 266 nm in a reaction cell under slow-flow conditions and time-resolved detection of OH by LIF. The evaluation of the pseudo-first-order decays gives directly the rate coefficient of the OH loss (OH reactivity) or inverse OH lifetime. Organic compounds were measured by a Proton-Transfer-Reaction-Time-Of-Flight Mass-Spectrometry instrument (PTR-TOF-MS), nitrogen oxides and ozone by chemiluminescence instruments and nitrous acid by a Long Path Absorption Photometer (LOPAP). During one of the experiments, peroxyacyl nitrates, PAN and MPAN, which serve as reservoirs for peroxy radicals and nitrogen oxides during MACR oxidation, were detected by gas chromatography (GC).

2.3 Model calculations

Time series of measurements were compared to calculations using the Master Chemical Mechanism version 3.2 (MCM) (Jenkin et al., 1997; Saunders et al., 2003) available at <http://mcm.leeds.ac.uk/MCM>. The MCM represents the current knowledge of atmospheric chemistry. In addition to the chemistry from the MCM, chamber specific properties were included in the model calculations. Dilution of trace gases due to the replenishment of zero air was modelled from monitored rates of the dilution flow. The dependence of source strengths for HONO, HCHO and CH₃CHO on radiation, relative humidity and temperature were taken from parameterizations described earlier (Rohrer et al., 2005; Karl et al., 2006). The source strengths were scaled, in order to match formation of NO_x, HCHO and CH₃CHO during the zero air part of the experiment. The part of the OH reactivity (approximately 1 s⁻¹) which could not be explained by the presence of measured OH reactants was treated as an OH reactant of constant concentration, which converts OH to HO₂ like CO does. The value of this “background” OH reactivity was determined from the measured OH reactivity at the start of the experiment (dark chamber), when only zero air and water vapour was present. Also RO₂ radicals were formed in the sunlit chamber from unknown sources. A photolytic RO₂ source was implemented in the model, which was similarly parameterized as the

5203

empirical functions for the HONO and HCHO sources. The applicability of this procedure was confirmed in test experiments, for which the production rate was scaled to match measured RO₂ concentrations.

The model was constrained by measurements of temperature, pressure, calculated dilution rates, measured water vapour mixing ratios, and photolysis frequencies for NO₂, HCHO, O₃, MACR and HONO. Photolysis frequencies and relative humidity constrained the calculated chamber sources for HONO, HCHO, and CH₃CHO. Photolysis frequencies that were not measured were first calculated by a MCM (version 3.1) function for clear sky conditions and then scaled by the ratio of the measured and calculated NO₂ photolysis frequencies to account for reductions of the solar radiation by clouds and the transmission of the Teflon film. Constrained parameters were re-initialized on a 1 min time grid. The injection of trace gases (O₃, MACR) was modelled as sources, which were turned on for the time of the injection. The source strength for ozone was adjusted to match the measured concentrations right after the injection and that for MACR was adjusted to match the change in the measured OH reactivity. Otherwise, trace gas concentrations were calculated by the model.

Modelled HO₂ concentrations presented here are the sum of calculated HO₂ and a fraction of specific RO₂ that are an interference in the HO₂ measurements (like introduced by Lu et al., 2012, as HO₂^{*}), so that measurements can be compared to calculations. Model calculations taking RO₂ conversion efficiency from characterization experiments of the instrument suggest that the contribution of this interference to the entire HO₂ detection was less than 5 % for these experiments. Calculated RO₂ concentrations that are shown in the following only include those RO₂ species that are efficiently converted to OH in the RO₂ measurement channel of the LIF instrument.

3 Results and discussion

3.1 Time series of trace gas concentrations

Once the humidified clean air is exposed to sunlight, HONO is formed on the chamber walls. Its photolysis increases the concentrations of NO_x and OH (Fig. 1). During this initial phase of the experiment, the OH reactivity is only approximately 1 s⁻¹, so that maximum OH concentrations of 1 × 10⁷ cm⁻³ are reached (OH concentrations in Fig. 1 are scaled by a factor of 0.5 during this part of the experiment). MACR injections increase the OH reactivity to up to 13.5 s⁻¹, so that OH concentrations drop to (1–1.5) × 10⁶ cm⁻³. The maximum MACR mixing ratio after the last injection is 14 ppbv. OH dominantly reacts with MACR during the entire experiment (e.g. 14 ppbv MACR corresponds to an OH reactivity of 10 s⁻¹). Reaction of OH with MACR initiates a reaction chain that produces RO₂ and HO₂, which includes reactions with NO, so that RO₂ and HO₂ concentrations increase in the presence of MACR. Similarly, concentrations of radical reservoir species peroxyacetyl nitrate and peroxy methacryloyl nitrate, PAN and MPAN (Table 3), are increasing after each MACR injection. These species are products of the reaction of acyl peroxy radicals with NO₂. MPAN and PAN are thermally unstable (Roberts and Bertman, 1992), so that a thermal equilibrium is established. Because PAN is also formed from acetaldehyde in the sunlit chamber, the PAN mixing ratio starts increasing before MACR is injected. The NO concentration is nearly constant over the course of the experiment with a mixing ratio of approximately 90 pptv.

Model calculations applying MCM give OH concentrations, which are approximately 50 % lower than measurements during the MACR oxidation part of the experiment (Fig. 1). The increasing difference between measured and modelled MACR indicates that less MACR is oxidized in the model during the experiment supporting that OH concentrations in the chamber are indeed larger than calculated.

The reaction of OH with MACR produces three RO₂ species (MCM names: MACRO2, MACROHO2, MACO3, Table 3). Measured RO₂ radical concentrations are reproduced by model calculations. Acyl peroxy radicals like MACO3 are detected

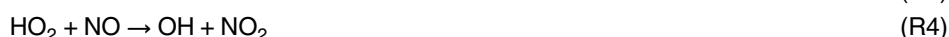
5205

by the LIF instrument with low sensitivity (see above). However, the good model-measurement agreement of MPAN and PAN mixing ratios, which are formed from MACO3, indicates that model calculations reproduce MACO3 concentrations. HO₂ concentrations are slightly underestimated, but the difference is within the uncertainty of measurements (Table 2).

In general, the description of radical species by MCM during the initial phase of the experiment is expected to be less accurate, because (1) the OH reactivity is mostly caused by unknown species and (2) radical sources and sinks are not well-defined. After the initial phase of the experiment the OH reactivity is dominated by MACR. Then, a much better model-measurement agreement can be expected, provided the underlying mechanism is correct, because chamber specific properties like the small OH reactivity from unknown species do not any longer play a role. This has been shown in similar experiments, when CO or butene was the dominant OH reactant. A model-measurement agreement for radical species within 30 % can be achieved in these reference experiments.

3.2 OH budget analysis

The significant underprediction of the measured OH concentration in the presence of MACR in the chamber experiments (Fig. 1) and the relative good agreement of the measured and modelled OH reactivity suggest a missing OH source in the model. The missing production rate can be analyzed by a model independent approach by comparing the OH production and destruction rates of known processes (Hofzumahaus et al., 2009). Primary OH sources in the chamber are O₃ and HONO photolysis. Furthermore, OH is produced from radical recycling via the reaction of HO₂ with NO:



All three contributions to the entire OH production rate can be calculated using only experimental data. Also the OH reactivity and the OH concentration were measured, so that the OH destruction rate can be calculated. Figure 2 shows time series of the OH production (summed up as coloured areas) and of the OH destruction rate for the experiment on 11 August 2011. Before MACR is injected to the chamber air, the OH production is balanced by its destruction as expected for a short-lived species like OH under steady-state conditions. However, during the MACR oxidation part of the experiment the calculated OH destruction rate is on average twice as large as the sum of OH production from radical recycling via the $\text{HO}_2 + \text{NO}$ reaction and O_3 and HONO photolysis. The grey shaded area in Fig. 2 indicates the additional OH production from an unknown source that is needed to balance the OH destruction (“missing OH source”). Apparently, the missing OH source is linked with the degradation of MACR by OH.

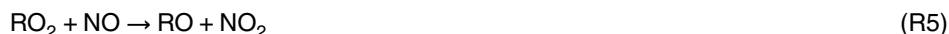
In the following, the data from all experiments are collectively analyzed to determine the missing OH source. This is justified because conditions of the experiments were similar (Table 1). The time-resolved missing OH source shows considerable variability over the course of all experiments, but no significant trend with time is seen in the data (Fig. 3, upper panel). This indicates that the additional OH is most likely not produced from longer-lived first-generation organic products of the MACR oxidation such as hydroxyacetone. These products would accumulate over the course of the experiment because they are less reactive towards OH (Butkovskaya et al., 2006). Therefore, an increasing OH production would be expected, if there was additional OH produced from these species.

Part of the variability of the time series of the missing OH production rate is caused by the variability of the production rate of RO_2 formed in the reaction of MACR with OH (Fig. 3). Here, the RO_2 production rate is calculated from measured OH and MACR concentrations assuming that every reaction of OH with MACR yields one RO_2 radical. Plotting the missing OH production rate against the RO_2 formation rate (Fig. 3) reveals a clear correlation between both values. This suggests that OH is formed from an RO_2 reaction channel missing in the MCM mechanism. The slope of the correlation would

5207

be the amount of OH that is additionally produced from each RO_2 radical. A weighted linear fit with a fixed zero offset gives a value of 0.77 ± 0.3 . Here, the uncertainty of ± 0.3 is determined by the accuracy of measurements that are included in both coordinates of the correlation (Fig. 3) giving an uncertainty of the slope of approximately $\pm 40\%$.

This additional reaction channel competes with the reaction of RO_2 with NO, which finally also regenerates OH, and the reaction of RO_2 with HO_2 , which is a radical termination reaction forming peroxides (ROOH):



The additional OH yield of the source of 0.77 ± 0.3 OH per RO_2 that is required to close the OH budget can be regarded as the branching ratio of the last reaction. The large value indicates that this reaction channel is an important pathway for conditions of these experiments (NO mixing ratios less than 100 pptv and HO_2 concentrations less than $6 \times 10^8 \text{ cm}^{-3}$).

3.3 Modifications of the MACR oxidation scheme

3.3.1 Generic OH recycling with X

A large discrepancy between measured and modelled OH concentrations has been observed in several field campaigns. In order to explain the high OH concentrations in some field campaigns, a generic recycling of OH radicals by a constant amount of an unknown compound X was assumed that would convert peroxy radicals to OH like NO does, but without accompanying ozone production (Hofzumahaus et al., 2009; Lu et al., 2012, 2013):



5208

Different amounts of X (in units of NO equivalents) were required: Pearl-River-Delta 800 pptv (Hofzumahaus et al., 2009; Lu et al., 2012), Beijing 400 pptv (Lu et al., 2013), and Borneo 700 pptv (Whalley et al., 2011). The nature of X, however, remained unclear, so that this mechanism could only serve as an empirical description. Recently, generic OH recycling was also applied, in order to describe fast OH regeneration from isoprene oxidation by OH in experiments in the SAPHIR chamber (Fuchs et al., 2013). A constant NO equivalent of 100 pptv was required in this case. It was shown that the effect of a generic OH recycling by X had the same effect as OH production from RO₂ radical isomerization and decomposition reactions.

Generic OH recycling by X is also tested for MACR oxidation experiments here, in order to see, if this empirical mechanism can also describe observations like shown for isoprene oxidation experiments. In fact, all observations including those of OH and MACR can be reproduced, if the mixing ratio of X is assumed to be equivalent to 50 pptv NO (Figs. 4 and 5). This amount of X is only half of what was found for isoprene oxidation for similar conditions (Fuchs et al., 2013) and is approximately ten times smaller compared to the amount of X that was needed to explain the above mentioned field observations.

3.3.2 RO₂ isomerization reactions.

The reaction of OH with MACR either leads to OH addition to the C=C double bond or H-abstraction from the CHO group (Tuazon and Atkinson, 1990; Orlando et al., 1999). OH adds dominantly to the external olefinic carbon atom (yield MCM: 47 %, Fig. 6) forming an RO₂ radical after reaction with O₂ (MCM: MACRO2). OH addition to the internal carbon atom is less likely (yield MCM: 8 %) and forms a different RO₂ radical after reaction with O₂ (MCM: MACROHO2). H-abstraction from the CHO group of MACR leads to the formation of an acyl peroxy radical after reaction with O₂ (MCM: MACO3, yield 45 %, Fig. 6).

Recent work has shown that the yield of OH from the reaction of HO₂ with acyl peroxy radicals like MACO3 could be larger than thought before (Dillon and Crowley,

5209

2008; Taraborrelli et al., 2012). The chemical model MCM used in this work assumes an OH yield of 0.44 for the reaction of HO₂ with MACO3, whereas a yield of 0.7 was found for the simplest acyl peroxy radical CH₃CO₃ (Dillon and Crowley, 2008). Although the qualitative behaviour of the missing OH source would be consistent with a larger OH yield from the reaction of HO₂ with MACO3 (Fig. 3), the turnover rate of this reaction is too small, in order to significantly increase the OH production rate. Doubling of the OH yield would increase the OH production rate by less than 0.1 ppbv h⁻¹, much smaller than the missing OH production rate.

Quantum chemical calculations showed that RO₂ isomerization with subsequent decomposition could lead to a fast OH regeneration from RO₂ from isoprene via 1,5-H-shift or 1,6-H-shift isomerization with subsequent decomposition of the products (Peeters et al., 2009; Peeters and Müller, 2010; da Silva et al., 2010). Similar reaction schemes have also been proposed for MACR (Peeters et al., 2009; Crounse et al., 2012; Asatryan et al., 2010; da Silva, 2012). A 1,5-H-shift for MACRO2 with subsequent decomposition would produce methylglyoxal, formaldehyde and OH, but an only small reaction rate constant of less than 0.008 s⁻¹ at 303 K has been calculated (Peeters et al., 2009; Crounse et al., 2012). Because additional OH from this isomerization reaction applies only for one RO₂ isomer (MACRO2) from the OH + MACR reaction and the rate constant is relatively small, the amount of additional OH from this isomerization channel is rather small. Time series of modelled radical and trace gas concentrations are shown in Fig. 4 for this case and Fig. 5 displays the ratio of measured to modelled OH concentrations. The 1,5-H-shift alone only slightly improves the model-measurement agreement.

In addition to the 1,5-H-shift of MACRO2, a much faster 1,4-H-shift for MACRO2 and a fast 1,5-H-shift for MACROHO2 with an isomerization rate constant of $(0.5 \pm 0.3) \text{ s}^{-1}$ at 296 K for both reactions have been suggested (Crounse et al., 2012). The 1,5-H-shift of MACROHO2 would produce hydroperoxyacetone (MCM: HYPERACET, Table 3), CO and HO₂. The 1,4-H-shift of MACRO2 would lead to the formation of hydroxyacetone, CO and OH (Crounse et al., 2012) (Fig. 6). A laboratory study (Crounse et al.,

2012) shows that hydroxyacetone concentrations, which were measured in MACR oxidation experiments with low NO concentrations, are much larger than expected. According to this study this result is consistent with the fast production of hydroxyacetone in the 1,4-H-shift isomerization channel of MACRO2. Application of a temperature dependence as suggested in literature (Crounse et al., 2012) yields a rate constant of 0.66 s^{-1} at the temperature during the experiment on 11 August 2011 (301 K). For conditions of this experiment, more than 95 % of the MACRO2 would undergo the 1,4-H-shift. Also the branching ratio of the 1,5-H-shift for MACROHO2 would be 95 %, if the reaction rate constant was similarly large as suggested. Figure 4 shows time series of concentrations and Fig. 5 the ratio of measured to modelled OH concentrations (case B), if both, the 1,4-H-shift of MACRO2 and the 1,5-H-shift of MACROHO2, are included. All observations, especially OH concentrations, are matched in this case. Most of the additional OH is formed by the 1,4-H-shift reaction of MACRO2. At the end of the experiment, the isomerization mechanism is expected to increase the hydroxyacetone mixing ratio by 1.5 ppbv compared to MCM calculations (Fig. 4).

Sensitivity model calculations with variation of the 1,4-H-shift isomerization rate constant were performed to estimate the sensitivity of calculated OH concentrations for experiments here. Decreasing the isomerization rate to a value, for which the median of the difference between measured and modelled OH has a maximum value of 30 % (the agreement that is expected from reference experiments), gives a lower limit of the rate constant constant of 0.03 s^{-1} , for which model calculations would be still consistent with the observations. In this case, the MACRO2 isomerization reaction would regenerate 50 % of the OH radicals that were consumed in the MACR+OH reaction to produce MACRO2. In contrast, modelled OH concentrations are insensitive to larger a reaction rate constant than suggested in literature (Crounse et al., 2012), because MACRO2 radicals already nearly exclusively undergo isomerization at conditions of this experiment, if the literature value is applied (Fig. 6). In this case, the yield of OH regenerated by isomerization is limited by the yield of MACRO2 from the reaction of MACR with OH. In fact, the MCM predicted MACRO2 yield of 0.47 is consistent with our experimental

5211

yield of 0.77 ± 0.3 OH, if complete MACRO2 to OH recycling via the isomerization reaction is assumed. Therefore, these experiments do not allow to determine a higher limit of the 1,4-H-shift isomerization rate constant.

Besides thermal decomposition of RO_2 another reaction scheme has been proposed from quantum-chemical calculations (da Silva, 2012; Asatryan et al., 2010). This suggests that the vibrationally excited adduct of MACR and OH reacts with O_2 on a similar time-scale as collisional deactivation of the adduct takes place. As a consequence, approximately 20 % of the MACR-OH adduct would react with O_2 and would form “double activated” RO_2 radicals, which then can decompose (da Silva, 2012). Decomposition of the “double activated” RO_2 would lead to the formation of either methylglyoxal, formaldehyde and OH or hydroxyacetone, CO and OH. In the result, this mechanism is equivalent to the 1,4- and 1,5-H-shift isomerization reactions (Table 4) and would be equivalent to a maximum isomerization rate constant of 0.007 s^{-1} , in order to yield a branching ratio of maximum 20 % for conditions of these experiments. As shown above, more than 50 % of MACRO2 needs to immediately regenerate OH, in order to explain our observations, much larger than the 20 % yield of “double activated” RO_2 . Therefore, this mechanism alone is not sufficient to bring calculations and measurements into agreement. Nevertheless, part of the discrepancy could be potentially due to the decomposition of “double-activated” RO_2 , because it is not possible to distinguish both mechanisms in our experiments.

The 1,4-H-shift isomerization rate constant that is required to explain observations from MACRO2 isomerization ($> 0.03 \text{ s}^{-1}$) is equivalent to the reaction of MACRO2 with more than 150 pptv NO. This value is larger than the amount of X that is needed to describe measured OH concentrations in the “X”-mechanism (see above). In the “X”-mechanism 50 pptv X is equivalent to an additional RO_2 loss rate of 0.01 s^{-1} . However, in the “X”-mechanism, additional OH is recycled by all RO_2 species, so that the overall impact is larger than that from MACRO2 alone. Therefore, the 1,4-H-shift isomerization rate constant cannot be directly compared to the loss rate of MACRO2 with X in the “X”-mechanism.

5212

4 Summary and conclusions

Measured OH concentrations during MACR oxidation experiments in the atmosphere simulation chamber SAPHIR are underestimated by chemical models by approximately 50 % (NO mixing ratios approximately 90 pptv, HO₂ concentrations approximately $5 \times 10^8 \text{ cm}^{-3}$ and $T = 301 \text{ K}$). The analysis of the OH budget reveals that an additional OH source is required to balance the measured OH destruction rate. Experiments allow to constrain the overall strength of the OH source regardless of the exact chemical mechanism that is responsible for the OH production.

Potential mechanisms behind the missing OH source can be the production of OH from unimolecular isomerization and decomposition reactions of RO₂ radicals (Peeters et al., 2009; Crounse et al., 2012; Asatryan et al., 2010; da Silva, 2012) and the decomposition of double activated RO₂ (Asatryan et al., 2010; da Silva, 2012) both giving the same products. All mechanisms would enhance OH by producing OH from RO₂ without reactions with NO, consistent with observations here. However, only the 1,4-H-shift (Crounse et al., 2012) would be strong enough to bring observations and calculations into agreement, whereas the 1,5-H-shift and decomposition of double activated RO₂ would only slightly improve the agreement between model calculations and measurements. Model calculations are consistent with the observations within the expected agreement, if the reaction rate constant for the 1,4-H-shift of the RO₂ isomer MACRO2 is larger than 0.03 s^{-1} . In this case, at least 50 % of MACRO2 undergoes the 1,4-H-shift reaction instead of reacting with NO or HO₂ as assumed in chemical models like the MCM. The 1,4-H-shift reaction would be competitive to the reaction of MACRO2 with minimum 150 pptv NO.

A yield of 0.77 ± 0.3 for additionally produced OH is found from the OH budget analysis in these experiments. It is maximum 0.55, if unimolecular RO₂ reactions of MACRO2 and MACROHO2 are responsible for the additional OH as suggested by Crounse et al. (2012). This value is comparable to the overall yield of OH from unimolecular RO₂ reactions produced from isoprene-derived RO₂ (38–45 %) for similar

5213

conditions (Fuchs et al., 2013). However, the impact of these reaction pathways is less for MACR compared to isoprene for two reasons: (1) typical MACR mixing ratios are smaller compared to isoprene, because MACR is a product of isoprene degradation with a yield of less than 30 % (Galloway et al., 2011) and (2) its reaction rate constant with OH is 3.5 times smaller, so that the MACR oxidation rate and therefore the production rate of MACR derived RO₂ is smaller.

During field campaigns in the Amazonian rainforest, when unexpected large OH was found, isoprene was the dominant OH reactant and therefore also substantial amounts of MACR were present (Kubistin et al., 2010). Only the sum of MVK and MACR was measured. Assuming that at most half of the measured MVK + MACR concentration was MACR, MACR mixing ratios were only 20 % of the mixing ratio of isoprene, when the largest discrepancy between measured and predicted OH was found (Kubistin et al., 2010). Taking also the smaller reaction rate constant of MACR with OH into account, the contribution of additional OH from MACR oxidation was significant, but most likely much smaller compared to that from isoprene. Because additional OH production from isoprene alone can only explain a smaller part of the entire gap between measured and predicted OH (Fuchs et al., 2013), the contribution of additional OH from MACR derived RO₂ is most likely not large enough to close the remaining gap. During field measurements in China, MACR oxidation played only a minor role (Lou et al., 2010), so that the impact of additional OH recycling from MACR-derived RO₂ is rather small. Nevertheless, results here show that the class of RO₂ isomerization reactions plays an important role at atmospheric conditions with low NO concentrations.

Acknowledgements. This work was supported by the EU FP-7 program EUROCHAMP-2 (grant agreement no. 228335) and by the EU FP-7 program PEGASOS (grant agreement no. 265307). S. Nehr and B. Bohn thank the Deutsche Forschungsgemeinschaft for funding (grant BO 1580/3-1). The authors thank A. Buchholz, P. Schlag, F. Rubach, H.-C. Wu, S. Dixneuf, M. Vietz, P. Müssgen, and M. Bachner for additional measurements during this campaign and technical support. The authors also thank G. da Silva for helpful discussions.

5214

- tary boundary layer, *Atmos. Meas. Tech. Discuss.*, 2, 2027–2054, doi:10.5194/amtd-2-2027-2009, 2009. 5223
- Hausmann, M., Brandenburger, U., Brauers, T., and Dorn, H.-P.: Detection of tropospheric OH radicals by long-path differential-optical-absorption spectroscopy: Experimental setup, accuracy, and precision, *J. Geophys. Res.*, 102, 16011–16022, doi:10.1029/97jd00931, 1997. 5223
- Hofzumahaus, A., Rohrer, F., Lu, K., Bohn, B., Brauers, T., Chang, C.-C., Fuchs, H., Holland, F., Kita, K., Kondo, Y., Li, X., Lou, S., Shao, M., Zeng, L., Wahner, A., and Zhang, Y.: Amplified trace gas removal in the troposphere, *Science*, 324, 1702–1704, doi:10.1126/science.1164566, 2009. 5199, 5206, 5208, 5209, 5225
- Jenkin, M. E., Saunders, S. M., and Pilling, M. J.: The tropospheric degradation of volatile organic compounds: a protocol for mechanism development, *Atmos. Environ.*, 31, 81–104, 1997. 5203
- Jordan, A., Haidacher, S., Hanel, G., Hartungen, E., Märk, L., Seehauser, H., Schottkowsky, R., Sulzer, P., and Märk, T. D.: A high resolution and high sensitivity proton-transfer-reaction time-of-flight mass spectrometer (PTR-TOF-MS), *Int. J. Mass Spectrom.*, 286, 122–128, doi:10.1016/j.ijms.2009.07.005, 2009. 5223
- Karl, M., Dorn, H. P., Holland, F., Koppmann, R., Poppe, D., Rupp, L., Schaub, A., and Wahner, A.: Product study of the reaction of OH radicals with isoprene in the atmosphere simulation chamber SAPHIR, *J. Atmos. Chem.*, 55, 167–187, doi:10.1007/s10874-006-9034-x, 2006. 5203
- Kelly, T. J. and Fortune, C. R.: Continuous monitoring of gaseous formaldehyde using an improved fluorescence approach, *Int. J. Anal. Chem.*, 54, 249–263, 1994. 5223
- Kubistin, D., Harder, H., Martinez, M., Rudolf, M., Sander, R., Bozem, H., Eerdeken, G., Fischer, H., Gurk, C., Klüpfel, T., Königstedt, R., Parchatka, U., Schiller, C. L., Stickler, A., Taraborrelli, D., Williams, J., and Lelieveld, J.: Hydroxyl radicals in the tropical troposphere over the Suriname rainforest: comparison of measurements with the box model MECCA, *Atmos. Chem. Phys.*, 10, 9705–9728, doi:10.5194/acp-10-9705-2010, 2010. 5214
- Kuhn, U., Andreae, M. O., Ammann, C., Araújo, A. C., Brancaleoni, E., Ciccioli, P., Dindorf, T., Frattoni, M., Gatti, L. V., Ganzeveld, L., Kruijt, B., Lelieveld, J., Lloyd, J., Meixner, F. X., Nobre, A. D., Pöschl, U., Spirig, C., Stefani, P., Thielmann, A., Valentini, R., and Kesselmeier, J.: Isoprene and monoterpene fluxes from Central Amazonian rainforest inferred from tower-based and airborne measurements, and implications on the atmospheric chemistry and

5217

- the local carbon budget, *Atmos. Chem. Phys.*, 7, 2855–2879, doi:10.5194/acp-7-2855-2007, 2007. 5199
- Lelieveld, J., Butler, T. M., Crowley, J. N., Dillon, T. J., Fischer, H., Ganzeveld, L., Harder, H., Lawrence, M. G., Martinez, M., Taraborrelli, D., and Williams, J.: Atmospheric oxidation capacity sustained by a tropical forest, *Nature*, 452, 737–740, doi:10.1038/nature06870, 2008. 5199
- Lindinger, W., Hansel, A., and Jordan, A.: On-line monitoring of volatile organic compounds at pptv levels by means of proton-transfer-reaction mass spectrometry (PTR-MS) – Medical applications, food control and environmental research, *Int. J. Mass Spectrom.*, 173, 191–241, doi:10.1016/s0168-1176(97)00281-4, 1998. 5223
- Lou, S., Holland, F., Rohrer, F., Lu, K., Bohn, B., Brauers, T., Chang, C.-C., Fuchs, H., Häseler, R., Kita, K., Kondo, Y., Li, X., Shao, M., Zeng, L., Wahner, A., Zhang, Y., Wang, W., and Hofzumahaus, A.: Atmospheric OH reactivities in the Pearl River Delta – China in summer 2006: measurement and model results, *Atmos. Chem. Phys.*, 10, 11243–11260, doi:10.5194/acp-10-11243-2010, 2010. 5214, 5223
- Lu, K. D., Rohrer, F., Holland, F., Fuchs, H., Bohn, B., Brauers, T., Chang, C. C., Häseler, R., Hu, M., Kita, K., Kondo, Y., Li, X., Lou, S. R., Nehr, S., Shao, M., Zeng, L. M., Wahner, A., Zhang, Y. H., and Hofzumahaus, A.: Observation and modelling of OH and HO₂ concentrations in the Pearl River Delta 2006: a missing OH source in a VOC rich atmosphere, *Atmos. Chem. Phys.*, 12, 1541–1569, doi:10.5194/acp-12-1541-2012, 2012. 5199, 5201, 5204, 5208, 5209, 5223
- Lu, K. D., Hofzumahaus, A., Holland, F., Bohn, B., Brauers, T., Fuchs, H., Hu, M., Häseler, R., Kita, K., Kondo, Y., Li, X., Lou, S. R., Oebel, A., Shao, M., Zeng, L. M., Wahner, A., Zhu, T., Zhang, Y. H., and Rohrer, F.: Missing OH source in a suburban environment near Beijing: observed and modelled OH and HO₂ concentrations in summer 2006, *Atmos. Chem. Phys.*, 13, 1057–1080, doi:10.5194/acp-13-1057-2013, 2013. 5199, 5201, 5208, 5209
- Orlando, J. J., Tyndall, G. S., Fracheboud, J.-M., Estupiñán, E. G., Haberkorn, S., and Zimmer, A.: The rate and mechanism of the gas-phase oxidation of hydroxyacetone, *Atmos. Environ.*, 33, 1621–1629, doi:10.1016/s1352-2310(98)00386-0, 1999. 5209
- Peeters, J. and Müller, J.-F.: HO_x radical regeneration in isoprene oxidation via peroxy radical isomerisations, 2: experimental evidence and global impact, *Phys. Chem. Chem. Phys.*, 12, 14227–14235, doi:10.1039/C0CP00811G, 2010. 5199, 5210

5218

- Peeters, J., Nguyen, T. L., and Vereecken, L.: HO_x radical regeneration in the oxidation of isoprene, *Phys. Chem. Chem. Phys.*, 11, 5935–5939, doi:10.1039/b908511d, 2009. 5199, 5200, 5210, 5213, 5225
- Ren, X., Olson, J. R., Crawford, J. H., Brune, W. H., Mao, J., Long, R. B., Chen, Z., Chen, G., Avery, M. A., Sachse, G. W., Barrick, J. D., Diskin, G. S., Huey, L. G., Fried, A., Cohen, R. C., Heikes, B., Wennberg, P. O., Singh, H. B., Blake, D. R., and Shetter, R. E.: HO_x chemistry during INTEX-A 2004: observation, model calculation, and comparison with previous studies, *J. Geophys. Res.*, 113, D05310, doi:10.1029/2007JD009166, 2008. 5199
- Ridley, B. A., Grahek, F. E., and Walega, J. G.: A small, high-sensitivity, medium-response ozone detector suitable for measurements from light aircraft, *J. Atmos. Ocean. Tech.*, 9, 142–148, doi:10.1175/1520-0426(1992)009<0142:ASHSMR>2.0.CO;2, 1992. 5223
- Roberts, J. M. and Bertman, S. B.: The thermal decomposition of peroxyacetic nitric anhydride (PAN) and peroxyethacrylic nitric anhydride (MPAN), *Int. J. Chem. Kin.*, 24, 297–307, doi:10.1002/kin.550240307, 1992. 5205
- Rohrer, F. and Brüning, D.: Surface NO and NO₂ mixing ratios measured between 30° N and 30° S in the Atlantic region, *J. Atmos. Chem.*, 15, 253–267, 1992. 5223
- Rohrer, F., Bohn, B., Brauers, T., Brüning, D., Johnen, F.-J., Wahner, A., and Kleffmann, J.: Characterisation of the photolytic HONO-source in the atmosphere simulation chamber SAPHIR, *Atmos. Chem. Phys.*, 5, 2189–2201, doi:10.5194/acp-5-2189-2005, 2005. 5201, 5203
- Saunders, S. M., Jenkin, M. E., Derwent, R. G., and Pilling, M. J.: Protocol for the development of the Master Chemical Mechanism, MCM v3 (Part A): tropospheric degradation of non-aromatic volatile organic compounds, *Atmos. Chem. Phys.*, 3, 161–180, doi:10.5194/acp-3-161-2003, 2003. 5203
- Schlosser, E., Bohn, B., Brauers, T., Dorn, H.-P., Fuchs, H., Häseler, R., Hofzumahaus, A., Holland, F., Rohrer, F., Rupp, L. O., Siese, M., Tillmann, R., and Wahner, A.: Intercomparison of two hydroxyl radical measurement techniques at the atmosphere simulation chamber SAPHIR, *J. Atmos. Chem.*, 56, 187–205, doi:10.1007/s10874-006-9049-3, 2007. 5202, 5223
- Schlosser, E., Brauers, T., Dorn, H.-P., Fuchs, H., Häseler, R., Hofzumahaus, A., Holland, F., Wahner, A., Kanaya, Y., Kajii, Y., Miyamoto, K., Nishida, S., Watanabe, K., Yoshino, A., Kubistin, D., Martinez, M., Rudolf, M., Harder, H., Berresheim, H., Elste, T., Plass-Dülmer, C., Stange, G., and Schurath, U.: Technical Note: Formal blind intercomparison of OH measure-

5219

- ments: results from the international campaign HOxComp, *Atmos. Chem. Phys.*, 9, 7923–7948, doi:10.5194/acp-9-7923-2009, 2009. 5201, 5202
- Stone, D., Evans, M. J., Commane, R., Ingham, T., Floquet, C. F. A., McQuaid, J. B., Brookes, D. M., Monks, P. S., Purvis, R., Hamilton, J. F., Hopkins, J., Lee, J., Lewis, A. C., Stewart, D., Murphy, J. G., Mills, G., Oram, D., Reeves, C. E., and Heard, D. E.: HO_x observations over West Africa during AMMA: impact of isoprene and NO_x, *Atmos. Chem. Phys.*, 10, 9415–9429, doi:10.5194/acp-10-9415-2010, 2010. 5199
- Tan, D., Faloon, I., Simpas, J. B., Brune, W., Shepson, P. B., Couch, T. L., Summer, A. L., Carroll, M. A., Thornberry, T., Apel, E., Riemer, D., and Stockwell, W.: HO_x budget in a deciduous forest: results from the PROPHET summer 1998 campaign, *J. Geophys. Res.*, 106, 24407–24427, 2001. 5199
- Taraborrelli, D., Lawrence, M. G., Crowley, J. N., Dillon, T. J., Gromov, S., Grosz, C. B. M., Vereecken, L., and Lelieveld, J.: Hydroxyl radical buffered by isoprene oxidation over tropical forests, *Nat. Geosci.*, 5, 190–193, doi:10.1038/ngeo1405, 2012. 5199, 5210
- Tuazon, E. C. and Atkinson, R.: A product study of the gas-phase reaction of methacrolein with the OH radical in the presence of NO_x, *Int. J. Chem. Kin.*, 22, 591–602, doi:10.1002/kin.550220604, 1990. 5200, 5209
- Volz-Thomas, A., Xueref, I., and Schmitt, R.: An automatic gas chromatograph and calibration system for ambient measurements of PAN and PPN, *Environ. Sci. Pollut. Res.*, 4, 72–76, 2002. 5223
- Whalley, L. K., Edwards, P. M., Furneaux, K. L., Goddard, A., Ingham, T., Evans, M. J., Stone, D., Hopkins, J. R., Jones, C. E., Karunaharan, A., Lee, J. D., Lewis, A. C., Monks, P. S., Moller, S. J., and Heard, D. E.: Quantifying the magnitude of a missing hydroxyl radical source in a tropical rainforest, *Atmos. Chem. Phys.*, 11, 7223–7233, doi:10.5194/acp-11-7223-2011, 2011. 5199, 5209
- Wolfe, G. M., Thornton, J. A., Bouvier-Brown, N. C., Goldstein, A. H., Park, J.-H., McKay, M., Matross, D. M., Mao, J., Brune, W. H., LaFranchi, B. W., Browne, E. C., Min, K.-E., Wooldridge, P. J., Cohen, R. C., Crounse, J. D., Faloon, I. C., Gilman, J. B., Kuster, W. C., de Gouw, J. A., Huisman, A., and Keutsch, F. N.: The Chemistry of Atmosphere-Forest Exchange (CAFE) Model – Part 2: Application to BEARPEX-2007 observations, *Atmos. Chem. Phys.*, 11, 1269–1294, doi:10.5194/acp-11-1269-2011, 2011. 5199
- Wolfe, G. M., Crounse, J. D., Parrish, J. D., St. Clair, J. M., Beaver, M. R., Paulot, F., Yoon, T., Wennberg, P. O., and Keutsch, F. N.: Photolysis, OH reactivity and ozone reactivity of

5220

5221

Table 1. Experimental conditions of the MACR oxidation experiments. Maximum values are given for MACR and averaged values for the part of the experiment, when MACR was present, for the other parameters.

MACR ppbv	OH 10^6 cm^{-3}	NO _x ppbv	NO pptv	O ₃ ppbv	RH %	$j(\text{NO}_2)$ 10^{-3} s^{-1}	T K	date
14	2.5	0.8	90	40	40	4	301	11 Aug 2011
7	3.5	0.7	60	50	30	4	308	29 Aug 2012
9	3.5	0.6	70	40	45	4.5	302	6 Sep 2012

5222

Table 2. Instrumentation for radical and trace gas detection during the MACR oxidation experiments.

	Technique	Time Resolution	1 σ Precision	1 σ Accuracy
OH	DOAS ^a (Dorn et al., 1995; Hausmann et al., 1997; Schlosser et al., 2007)	205 s	$0.8 \times 10^6 \text{ cm}^{-3}$	6.5 %
OH	LIF ^b (Lu et al., 2012)	47 s	$0.3 \times 10^6 \text{ cm}^{-3}$	13 %
HO ₂ , RO ₂	LIF ^b (Fuchs et al., 2011)	47 s	$1.5 \times 10^7 \text{ cm}^{-3}$	16 %
k(OH)	Laser-photolysis + LIF ^b (Lou et al., 2010)	180 s	0.3 s^{-1}	0.5 s^{-1}
NO	Chemiluminescence (Rohrer and Brüning, 1992)	180 s	4 pptv	5 %
NO ₂	Chemiluminescence (Rohrer and Brüning, 1992)	180 s	2 pptv	5 %
O ₃	Chemiluminescence (Ridley et al., 1992)	180 s	60 pptv	5 %
MACR	PTR-TOF-MS ^c (Lindinger et al., 1998; Jordan et al., 2009)	30 s	15 pptv	14 %
HONO	LOPAP ^d (Häseler et al., 2009)	300 s	1.3 pptv	10 %
HCHO	Hantzsch monitor (Kelly and Fortune, 1994)	120 s	20 pptv	5 %
CH ₃ CHO	PTR-TOF-MS ^c (Lindinger et al., 1998; Jordan et al., 2009)	30 s	50 pptv	15 %
PAN, MPAN	GC ^e (Volz-Thomas et al., 2002)	600 s	25 pptv	10 %
Photolysis frequencies	Spectroradiometer (Bohn et al., 2005)	60 s	10 %	10 %

^aDifferential Optical Absorption Spectroscopy.

^bLaser Induced Fluorescence.

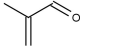
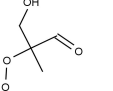
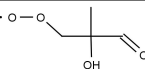
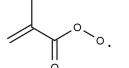
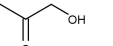
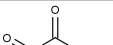
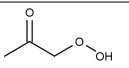
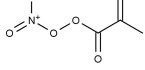
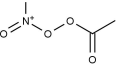
^cProton-Transfer-Reaction Time-Of-Flight Mass-Spectrometry.

^dLong Path Absorption Photometer.

^eGas Chromatography.

5223

Table 3. Chemical structure of MACR and products from its oxidation with OH. Acronyms are taken from the MCM.

MACR (methacrolein)	
MACRO2	
MACROHO2	
MACO3	
ACETOL (hydroxyacetone)	
MGLYOX (methylglyoxal)	
HYPERACET (hydroperoxyacetone)	
MPAN (peroxy methacryloyl nitrate)	
PAN (peroxyacetyl nitrate)	

5224

Table 4. Modification of MCM oxidation scheme for MACR. The “X”-mechanism adds generic recycling of OH via reaction of peroxy radicals with a compound X, which behaves like NO. The two cases of RO₂ isomerization produces additional OH via RO₂ isomerization with subsequent decomposition of the products.

	Reaction	Rate constant/s ⁻¹ cm ⁻³	Reference
X	HO ₂ + X → RO	$2.7 \times 10^{-12} \exp(360\text{K}/T)$	Hofzumahaus et al. (2009)
	RO ₂ + X → OH	$3.45 \times 10^{-12} \exp(270\text{K}/T)$	
RO ₂ isom. A	MACRO2 $\xrightarrow{1,5\text{-H-shift}}$ MGLYOX + OH + HCHO	0.008	Peeters et al. (2009)
RO ₂ isom. B	MACRO2 $\xrightarrow{1,4\text{-H-shift}}$ ACETOL + OH + CO	$2.9 \times 10^7 \exp(-5300\text{K}/T)$	Crounse et al. (2012)
	MACRO2 $\xrightarrow{1,5\text{-H-shift}}$ MGLYOX + OH + HCHO	0.0018	
	MACROHO2 $\xrightarrow{1,5\text{-H-shift}}$ HYPERACET + CO + HO ₂	0.5	

5225

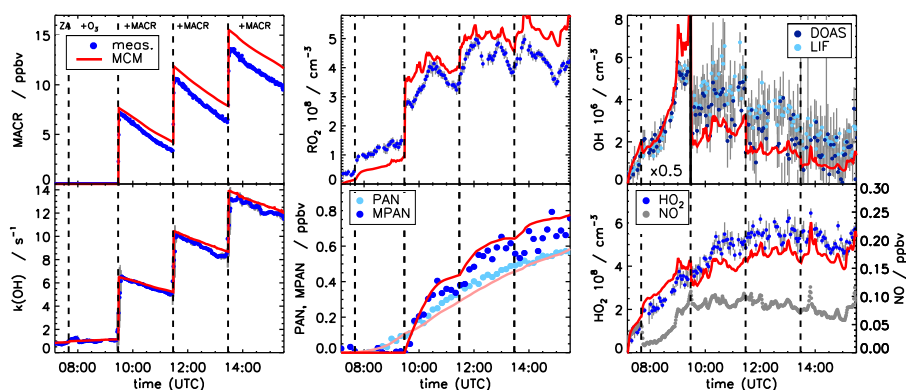


Fig. 1. Measured and modelled time series of MACR, $k(\text{OH})$, PAN, MPAN, RO₂, HO₂, OH and NO for the experiment on 11 August 2011. OH concentrations during the less important initial part (“ZA”, “+O₃”) of the experiment are scaled by a factor of 0.5. Model calculations applying MCM underestimate OH concentrations. Measured and modelled HO₂ concentrations include a small fraction of RO₂ radicals, which show up as an interference in the HO₂ detection (less than 5 % of the entire concentration). RO₂ radical concentrations shown here do not include the class of acyl peroxy radicals, which cannot be detected by the instrument.

5226

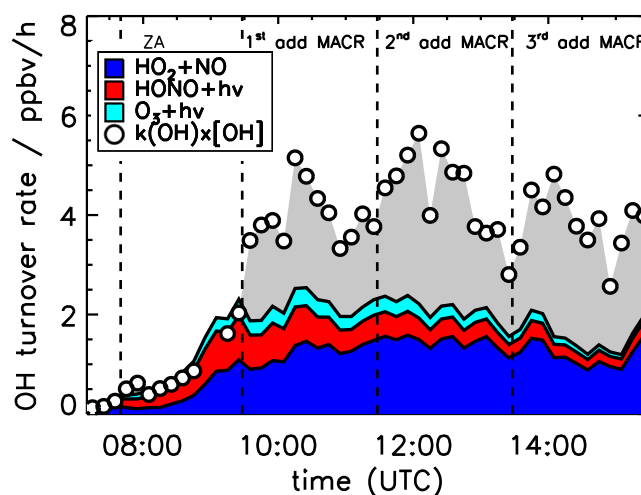


Fig. 2. OH budget for the experiment on 11 August 2011. Black circles give the turnover of the OH destruction rate calculated from measured OH concentrations (DOAS) and the measured OH reactivity. Coloured areas sum up the OH production from known sources ($\text{HO}_2 + \text{NO}$ reaction, O_3 and HONO photolysis), which can be calculated from measurements. Because of the short lifetime of OH the production and destruction rates are expected to be equal at all times. The gray area denotes the difference between destruction and production rate. Whereas the OH budget is closed before the injection of MACR (“ZA”), on average half of the OH source is missed during MACR oxidation.

5227

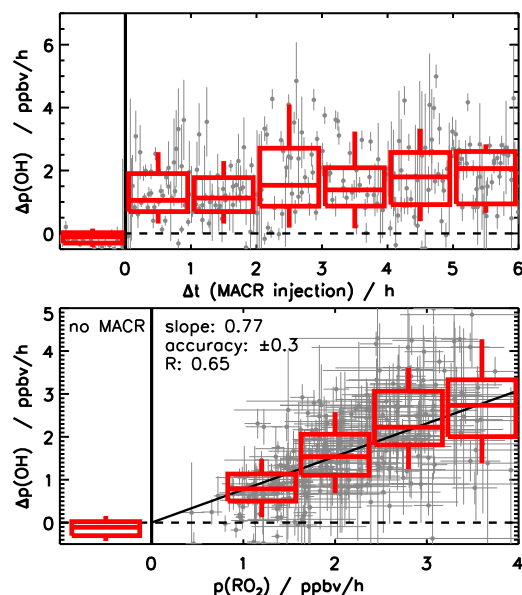


Fig. 3. Correlation between the missing OH source ($\Delta p(\text{OH})$) and (1) the time that has been elapsed since the first MACR injection (upper panel) and (2) production of RO_2 from the reaction of MACR and OH (lower panel). Grey dots give individual data points with statistical errors for all three experiments (Table 1), boxes show 25 and 75 % and whiskers 10 and 90 % percentiles. The value of the linear correlation coefficient of $R = 0.65$ shows the good correlation between the RO_2 production from MACR and the missing OH source. The slope of a weighted linear fit (black line) suggests that on average 0.77 OH radicals are immediately recycled from RO_2 for conditions of these experiments. The error of 0.3 is calculated from the accuracy of measurements.

5228

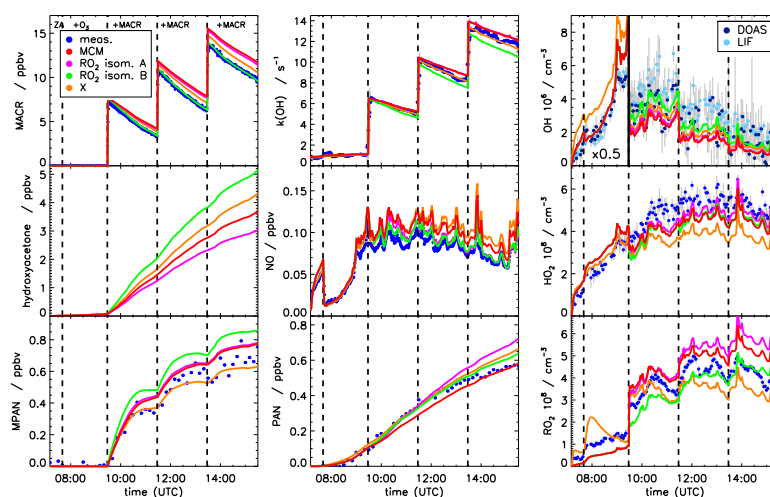


Fig. 4. Measured and modelled time series of MACR, $k(\text{OH})$, PAN, MPAN, RO_2 , HO_2 , OH and NO for the experiment on 11 August 2011. OH concentrations during the less important initial part of the experiment are scaled by a factor of 0.5. Different model runs were performed applying the pure MCM, MCM with two additional RO_2 isomerization reaction schemes (case A and B, see Table 4), and MCM with additional generic OH recycling ("X") with an NO equivalent of 50 pptv. Only calculated hydroxyacetone concentrations are shown, because it was not measured during experiments.

5229

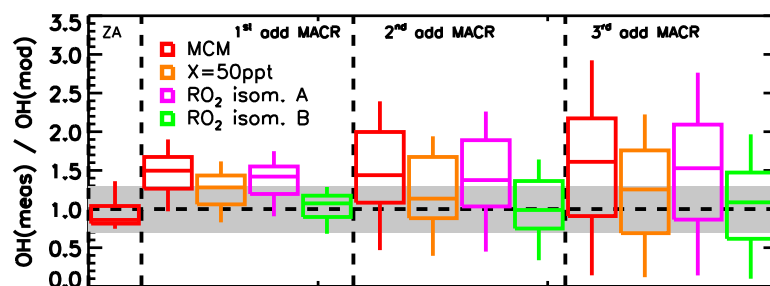


Fig. 5. Ratio of measured (DOAS) to modelled OH concentrations for the four parts of the experiment on 11 August 2011 applying different model approaches: MCM, MCM with additional generic OH recycling ("X"), and MCM with additional RO_2 isomerization schemes (case A and B, see Table 4). The grey shaded area gives the range of agreement of modelled and calculated OH concentrations that is achieved in reference experiments.

5230

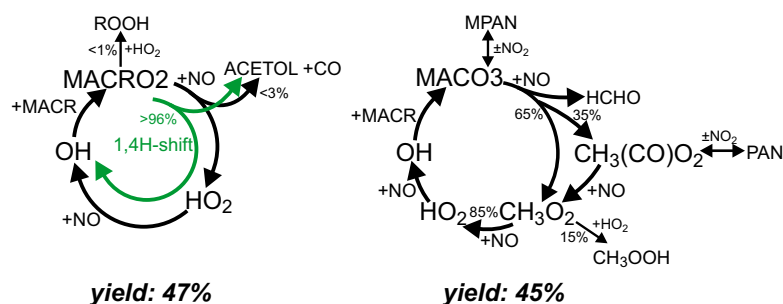


Fig. 6. Schematics of radical recycling from the reaction of MACR with OH taken from MCM (black arrows) showing the reactions which were of importance for conditions of these experiments. H-atom abstraction of the CHO group in MACR leads to the formation of an acyl peroxy radical (MACO3: yield 45 %), whereas OH addition to the C=C double bond forms two hydroxylalkoxy radical isomers (RO₂: MACRO2, yield 47 %, and MACROHO2, yield 8 % not shown here). Green arrows indicate the 1,4-H-shift reaction of MACRO2 (Crounse et al., 2012) (the less important 1,5-H-shift is not shown here). Branching ratios are given for conditions of the experiment on 11 August 2011 (NO = 90 pptv, HO₂ = 5 × 10⁸ cm⁻³, T = 301 K), if the fast unimolecular reaction is included.